



# The effects of wedge tail thickness on NACA 0021 airfoil performance

Md. Moynul Hasan<sup>1,\*</sup>, Md. Mashiur Rahaman<sup>1</sup>, N.M. Golam Zakaria<sup>1</sup>

## ARTICLE INFO

### Article history:

Received 19 Mar 2023;  
in revised from 26 Mar 2023;  
accepted 07 Apr 2023.

### Keywords:

NACA 0021, Wedge tail, CFD, Lift coefficient, Drag coefficient, Performance analysis.

© SEECMAR | All rights reserved

## ABSTRACT

In this study, the effects of the wedge tail thickness on the performance of the NACA 0021 airfoil were analyzed. The study employed RANS-CFD simulations in a two-dimensional domain to investigate the aerodynamic characteristics of the airfoils and evaluated the effects of Mach numbers ( $0.05 \leq M \leq 0.25$ ), Reynolds numbers ( $0.25 \times 10^6 \leq Re \leq 1 \times 10^6$ ), and angle of attack ( $1^\circ \leq \alpha \leq 9^\circ$ ) on their performance. Subsequently, the results were compared for all the airfoils, showing that the wedge tail increased the lift coefficient of the NACA 0021 airfoil, although it also increased the drag coefficient.

## 1. Introduction.

Airfoils are essential components in various engineering applications, particularly in aerospace Tuncer and Platzter (2000) and marine industries Sener and Aksu (2022); Fernández and Chakkor (2006), where they serve as control surfaces to regulate vehicle movement. Airfoils are commonly used on aircraft wings, such as ailerons, elevators, and flaps, to adjust lift and drag forces and control movement in different directions. Similarly, airfoils are used as control surfaces on rudders and fins to navigate ships and submarines in marine engineering. The primary purpose of control surfaces is to produce force, which helps regulate vehicle motion. While control surfaces may be fixed or movable, in the marine field, movable control surfaces are more prevalent, with the prime example being the ship rudder Molland (2011).

Implementing the Energy Efficiency Design Index (EEDI) can reduce carbon dioxide emissions and protect the global environment by decreasing ship speeds. Consequently, maneuverability in low-speed operations has gained significance, with marine rudders playing a pivotal role in ship navigation and maneuvering. Therefore, a growing demand for developing

high lift rudders are growing to improve ship maneuverability Nguyen and Ikeda (2016). One approach to achieving this is to enhance the cross-sectional design of the rudder Tasif and Karim (2017).

Various studies have been conducted on increasing lift force on lift surfaces, as discussed in textbooks such as Hoerner and Borst (1975) and Molland and Turnock (2011). One way to improve the performance of existing rudders is by adding a wedge tail to the NACA series Liu and Hekkenberg (2015). Wedge tail airfoil profiles have many practical applications in hydrodynamics Tasif and Karim (2017), particularly in shallow waters and at low speeds. Wedge tail rudders can extend the stall angle Liu and Hekkenberg (2015) and generate high lift coefficients, although they also cause additional drag Thieme (1965).

Previous studies by Van Nguyen and Ikeda (2013); Van and Yoshiho (2015); Van Nguyen and Ikeda (2014a, b); Nguyen and Ikeda (2014) have used the NACA 0024 airfoil section with a fishtail, wedge tail, and flat plate at the trail to develop high-lift rudders, showing an increase in lift coefficient with some increase in the drag coefficient. According to Van Nguyen and Ikeda (2014a), a fishtail with a small trailing edge and medium maximum thickness provides better hydrodynamics than others from the perspective of high lift, and low drag. Nguyen and Ikeda (2016) used NACA 0018 to analyze the effects of wedge tail on its performance and found a lift increase of up to 27% with some increase in drag. Additionally, Tasif and Karim

<sup>1</sup>Department of Naval Architecture & Marine Engineering, Bangladesh University of Engineering & Technology, Dhaka-1000, Bangladesh.

\*Corresponding author: Md. Moynul Hasan. E-mail Address: moynul0210@gmail.com.

(2017) analyzed the NACA 0012 airfoil section with a wedge tail and found up to a 15% increase in lift coefficient. They also analyzed the effects of a flap on the NACA 0012 airfoil section.

The NACA 0021 airfoil is one of the most thoroughly investigated and has various applications Rostamzadeh et al. (2013, 2014); Holst et al. (2019). Therefore, the effects of a wedge tail need to be analyzed on its performance at a low angle of attack.

## 2. Computational fluid dynamics analysis.

In this study, simulations were conducted on NACA 0021 and NACA 0021 wedge tail airfoils at a range of Mach numbers ( $0.05 \leq M \leq 0.25$ ), Reynolds numbers ( $0.25 \times 10^6 \leq Re \leq 1 \times 10^6$ ), and angle of attack ( $1^\circ \leq \alpha \leq 9^\circ$ ) using the Reynolds Averaged Navier-Stokes (RANS) method in a two-dimensional domain. The simulations were carried out using the commercial CFD software ANSYS Fluent, and high-quality meshes for the simulations were generated using ANSYS Mechanical. To validate the RANS method, a 2D NACA 0021 airfoil section with a chord length ( $c$ ) of 0.1524 m was used, to match the experimental setup conducted by Sheldahl and Klimas (1981).

### 2.1. Airfoil geometries.

The wedge tail airfoils presented in this study are based on the NACA 0021 airfoil profile, which exhibits a concave shape at 0.95c, and three different tail wedge thicknesses: 0.1c, 0.125c, and 0.15c. These values are presented in Table 1 and illustrated in Fig. 1.

Table 1: List of wedge tail sections.

Name	Trailing edge thickness
Wedge tail 01	0.1c
Wedge tail 02	0.125c
Wedge tail 03	0.15c

Source: Authors.

### 2.2. Governing equations.

The equations governing fluid flow problems are derived from physical laws and can be expressed mathematically. In particular, the equations for mass and momentum conservation are essential for describing fluid flow in any given case. As noted by Douvi et al. (2012), these equations can be represented as follows:

$$\frac{\partial \rho}{\partial t} + \nabla \cdot (\rho \vec{u}) = S_m, \quad (1)$$

$$\frac{\partial}{\partial t} (\rho \vec{u}) + \nabla \cdot (\rho \vec{u} \vec{u}) = -\nabla p + \nabla \cdot (\vec{\tau}) + \rho \vec{g} + \vec{F}, \quad (2)$$

where  $\vec{\tau}$  is the stress tensor, which can be written as:

$$\vec{\tau} = \mu \left[ \left( \nabla \vec{u} + \nabla \vec{u}^T \right) - \frac{2}{3} \nabla \cdot \vec{u} I \right]. \quad (3)$$

For steady and non-compressible two-dimensional flows, the continuity and momentum equations for viscous flow in the x and y directions are:

$$\frac{\partial u}{\partial x} + \frac{\partial v}{\partial y} = 0, \quad (4)$$

$$\rho \frac{Du}{Dt} = -\frac{\partial p}{\partial x} + \frac{\partial \tau_{xx}}{\partial x} + \frac{\partial \tau_{yx}}{\partial y} + \rho f_x, \quad (5)$$

$$\rho \frac{Dv}{Dt} = -\frac{\partial p}{\partial y} + \frac{\partial \tau_{xy}}{\partial x} + \frac{\partial \tau_{yy}}{\partial y} + \rho f_y. \quad (6)$$

In this study, the SST  $k - \omega$  turbulence model proposed by Menter (1994) has been utilized to account for turbulence effects in the simulation. This model is well suited for industrial applications, which combines the features of the standard  $k - \epsilon$  model in free flow with the Wilcox  $k - \omega$  model near walls. It has the same computational requirements as the Wilcox  $k - \omega$  model and low sensitivity to Reynolds number as the standard  $k - \epsilon$  model. Moreover, this model overcomes some of the limitations associated with these models, as pointed out by previous studies Frei (2017); Versteeg and Malalasekera (2007). As indicated by Suvanjumrat (2017), the SST  $k - \omega$  model consists of two equations expressed as follows:

$$\begin{aligned} \frac{\partial (\rho k)}{\partial t} + \text{div} (\rho k U_i) = \text{div} \left[ \left( \mu + \frac{\rho k}{\omega \sigma_k} \right) \nabla k \right] + \\ 2 \frac{\rho k}{\omega} S_{ij} \cdot S_{ij} - \frac{2}{3} \rho k \frac{\partial U_i}{\partial x_j} \delta_{ij} - \beta^* \rho k \omega, \end{aligned} \quad (7)$$

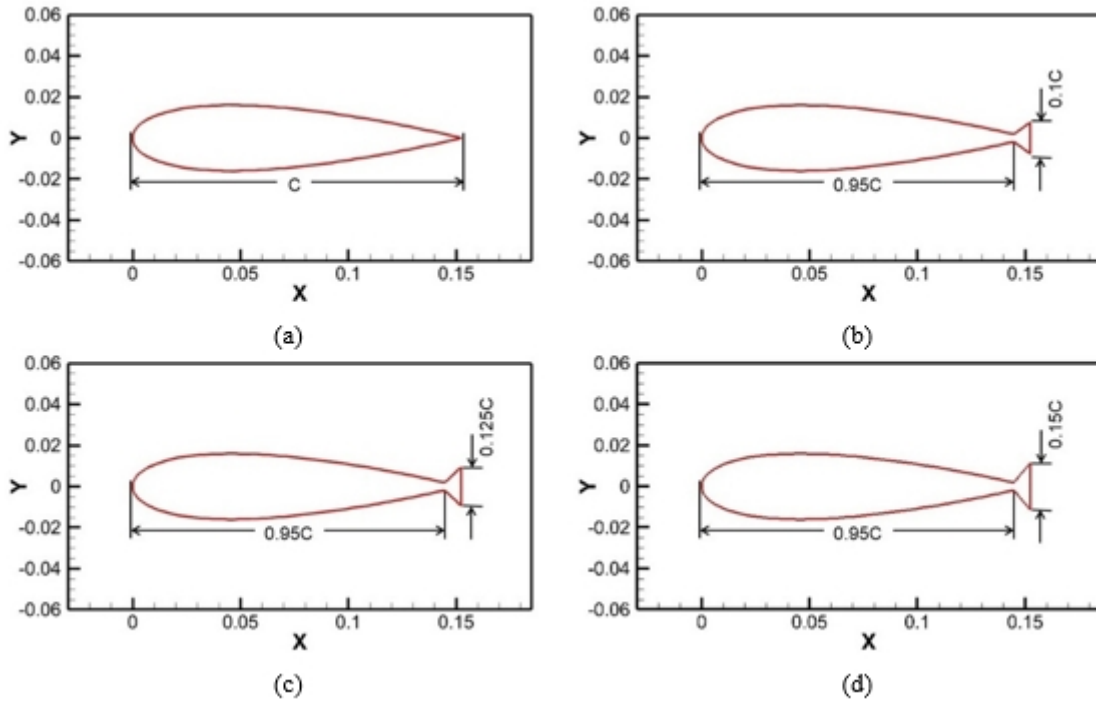
$$\begin{aligned} \frac{\partial (\rho \omega)}{\partial t} + \text{div} (\rho \omega U_i) = \text{div} \left[ \left( \mu + \frac{\rho k}{\omega \sigma_{\omega 1}} \right) \nabla \omega \right] \\ + 2 \rho \gamma_2 S_{ij} \cdot S_{ij} - \frac{2}{3} \rho \gamma_2 \omega \frac{\partial U_i}{\partial x_j} \delta_{ij} \\ - \beta_2 \rho \omega^2 + 2 \frac{\rho}{\omega \sigma_{\omega 2}} \frac{\partial k}{\partial x_k} \frac{\partial \omega}{\partial x_k}, \end{aligned} \quad (8)$$

where  $k$ ,  $\omega$ ,  $\nu$ , and  $y$  stand for turbulent kinetic energy, turbulent frequency, dynamic viscosity, and distance from the solid wall, respectively, and the values of  $\sigma_k$ ,  $\beta^*$ ,  $\sigma_{\omega 1}$ ,  $\gamma_2$ ,  $\beta_2$ , and  $\sigma_{\omega 2}$  are 1.0, 0.09, 2.0, 0.44, 0.083, and 1.17 respectively.

### 2.3. Boundary conditions.

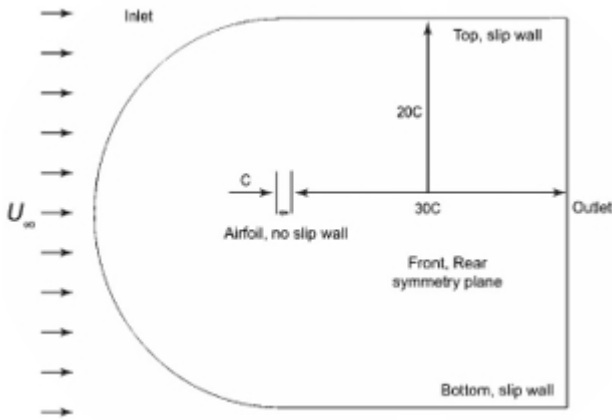
In this study, the inlet flow on the left side of the C-shaped domain was subjected to a uniform velocity, while slip boundary conditions were applied to the top and bottom walls. The outlet flow on the right side of the domain was controlled by atmospheric pressure. The front and rear domains were defined by a symmetry boundary condition, and only the airfoil profile wall was imposed with no-slip conditions ( $u_p = 0$ ). Simulations were conducted for an incompressible flow with a density of  $1.225 \text{ kg/m}^3$  and dynamic viscosity of  $1.7894 \times 10^{-5} \text{ kg/(ms)}$ , where the Reynolds numbers ( $Re$ ) ranged from  $0.25 \times 10^6$  to  $1 \times 10^6$ , and the Mach numbers ( $M$ ) was between 0.05 to 0.25. The airfoil domain and the corresponding boundary conditions are shown in Fig. 2.

Figure 1: Geometry of the (a) NACA 0021 (b) Wedge tail 01 (c) Wedge tail 02 (d) Wedge tail 03 airfoils.



Source: Authors.

Figure 2: Simulation of fluid flow around an airfoil in a C-type domain.

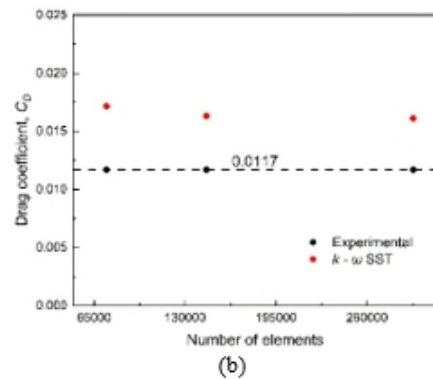
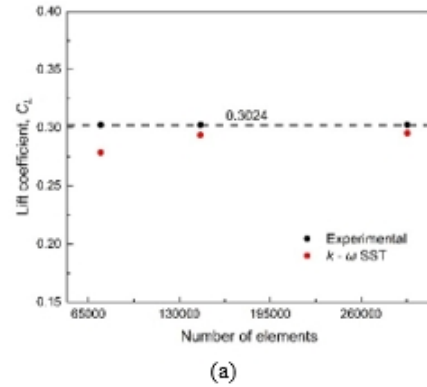


Source: Authors.

2.4. Mesh generation.

The size of the computational mesh has a significant impact on the accuracy of the numerical solution. Although increasing the number of mesh nodes can improve accuracy, it requires more computational resources and time. Therefore, the first step in the CFD simulation is to examine the effect of the mesh size on the solution outcomes. The impact of the number of mesh elements on the lift coefficient ( $C_L$ ) and drag coefficient ( $C_D$ ) for the NACA 0021 airfoil at an angle of attack ( $\alpha$ ) of  $3^\circ$ , where the Reynolds number ( $Re$ ) was set to  $3.6 \times 10^5$ , is presented in Fig. 3 and Table 2.

Figure 3: (a) Lift coefficient ( $C_L$ ) and (b) drag coefficient ( $C_D$ ) as a function of element number at  $3^\circ$  angle of attack ( $\alpha$ ) for NACA 0021 airfoil with a Reynolds number ( $Re$ ) of  $3.6 \times 10^5$ .



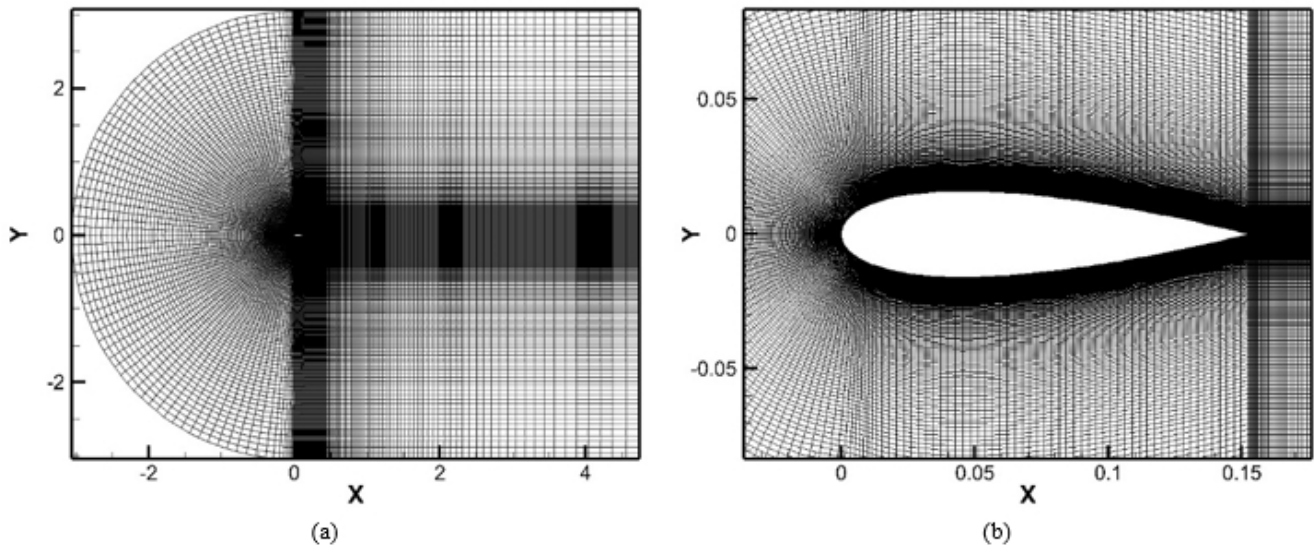
Source: Authors.

Table 2: Mesh independence study for a different number of elements on the surface of NACA 0021 airfoil with a Reynolds number ( $Re$ ) of  $3.6 \times 10^5$ .

Test case	No. of elements	Angle of attack, $\alpha$			
		$3^\circ$			
		$C_L$	% Deviation from Medium	$C_D$	% Deviation from Medium
Coarse	73800	0.27856	-5.17%	0.01715	-5.15%
<b>Medium</b>	<b>145200</b>	<b>0.29375</b>	<b>0.00%</b>	<b>0.01631</b>	<b>0.00%</b>
Fine	292988	0.29535	0.54%	0.01611	-1.23%

Source: Authors.

Figure 4: (a) Grid around NACA 0021 airfoil and (b) detail close to the NACA 0021 airfoil.



Source: Authors.

It was observed that a C-type grid with 145200 quadrilateral elements would suffice for a mesh-independent solution. The mesh resolution was increased to achieve higher computational precision in certain parts, such as around the airfoils. The near-wall cells on the upper and lower surfaces of the airfoil were adjusted to achieve a desired  $y^+$  value of 1, based on boundary layer theory, using the Pointwise<sup>®</sup>  $y^+$  calculator. According to boundary layer theory, the inner parts of the boundary layer must be resolved to a size of this  $y^+$ . The mesh around the NACA 0021 airfoil and associated near-body meshes are shown in Fig. 4.

### 3. Results and Discussion.

#### 3.1. Effects of the Mach number.

Five different Mach numbers were considered, namely  $M = 0.05, 0.1, 0.15, 0.2,$  and  $0.25$ , at a constant angle of attack of  $\alpha = 3^\circ$ . The impact of Mach number on velocity, pressure, lift coefficient, and drag coefficient for four different airfoils is presented in Figs. 5, 6, and 7, respectively. Fig. 7 shows that Wedge Tail 02 has the highest lift coefficient, increasing

with the Mach number. In contrast, NACA 0021 airfoil has the lowest drag coefficient, decreasing with an increase in Mach number. Additionally, the wedge tail thickness has a considerable effect on the lift coefficient and drag coefficient, as demonstrated in Fig. 8.

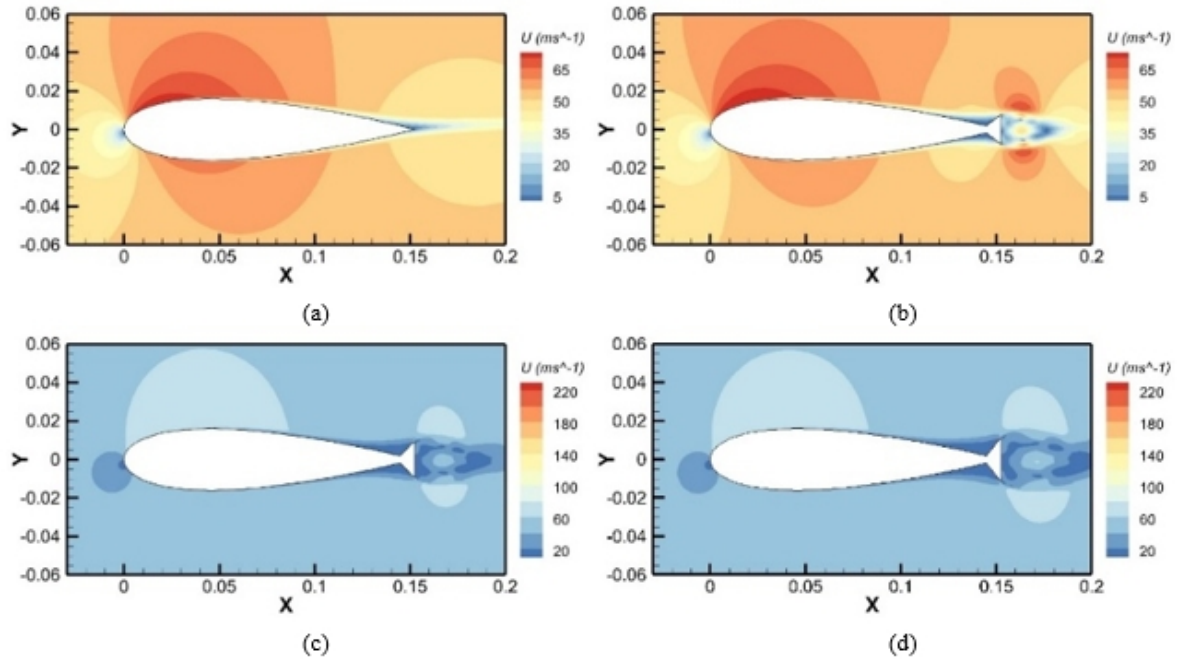
#### 3.2. Effects of the Reynolds number.

Five different Reynolds numbers were considered, namely  $Re = 0.25 \times 10^6, 0.4375 \times 10^6, 0.625 \times 10^6, 0.8125 \times 10^6$  and  $1 \times 10^6$ , at a constant angle of attack of  $\alpha = 3^\circ$ . The impact of Reynolds number on velocity, pressure, lift coefficient, and drag coefficient for four different airfoils is presented in Figs. 9, 10, and 11, respectively. Fig. 11 shows that Wedge Tail 02 has the highest lift coefficient, increasing with the Reynolds number. In contrast, NACA 0021 airfoil has the lowest drag coefficient, decreasing with an increase in Reynolds number. Additionally, the wedge tail thickness has a considerable effect on the lift coefficient and drag coefficient, as demonstrated in Fig. 12.

#### 3.3. Effects of the angle of attack.

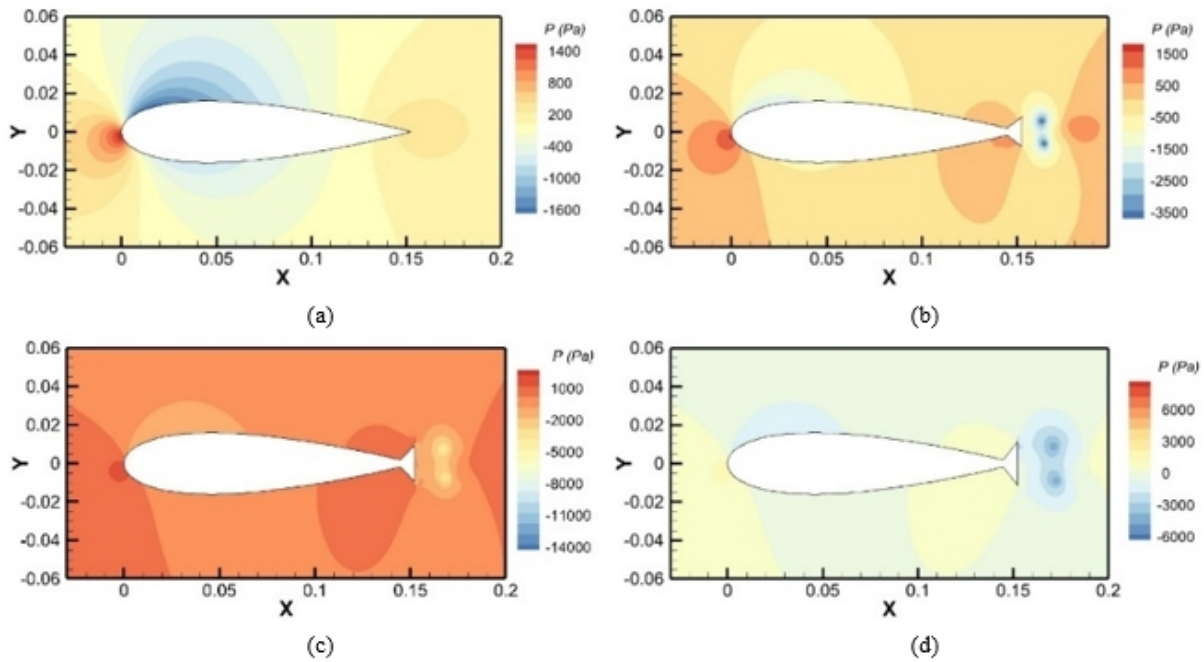
Five different angles of attack were considered, namely  $\alpha = 1, 3, 5, 7,$  and  $9$  at Reynolds number ( $Re$ ) of  $1 \times 10^6$ . The

Figure 5: Velocity contours of the (a) NACA 0021 (b) Wedge tail 01 (c) Wedge tail 02 (d) Wedge tail 03 airfoil at  $3^\circ$  angle of attack ( $\alpha$ ) with a Mach number ( $M$ ) of 0.15.



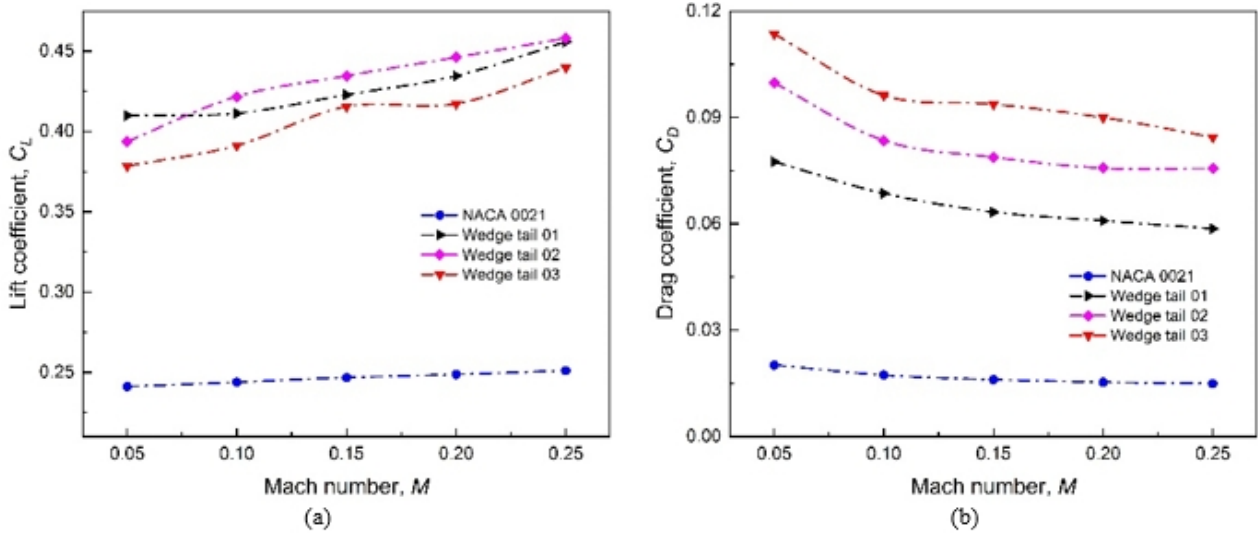
Source: Authors.

Figure 6: Pressure contours of the (a) NACA 0021 (b) Wedge tail 01 (c) Wedge tail 02 (d) Wedge tail 03 airfoil at  $3^\circ$  angle of attack ( $\alpha$ ) with a Mach number ( $M$ ) of 0.15.



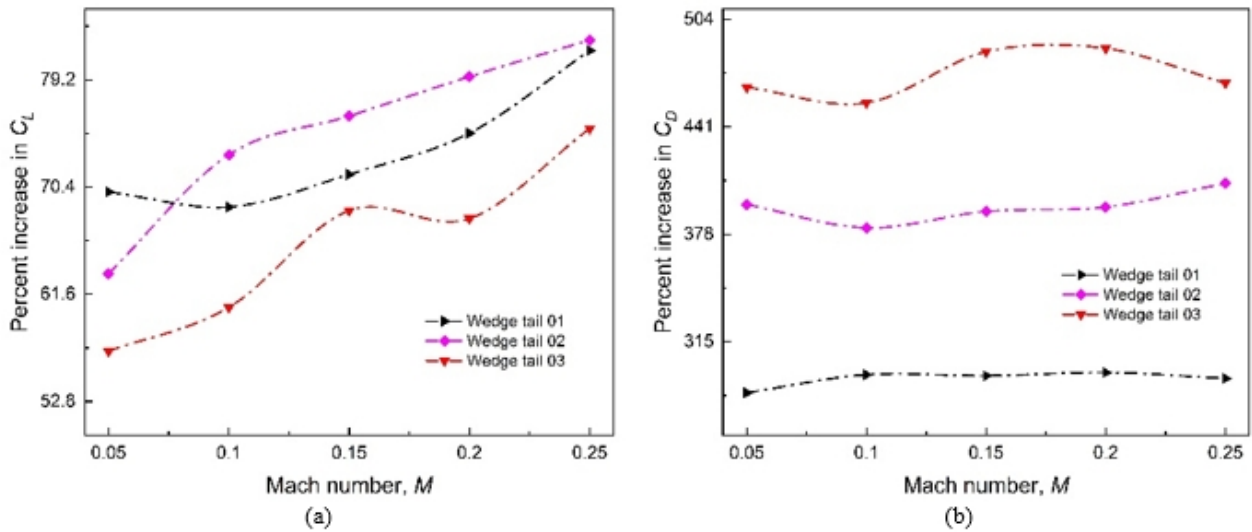
Source: Authors.

Figure 7: (a) Lift coefficient ( $C_L$ ) and (b) drag coefficient ( $C_D$ ) as a function of Mach number ( $M$ ) at  $3^\circ$  angle of attack ( $\alpha$ ).



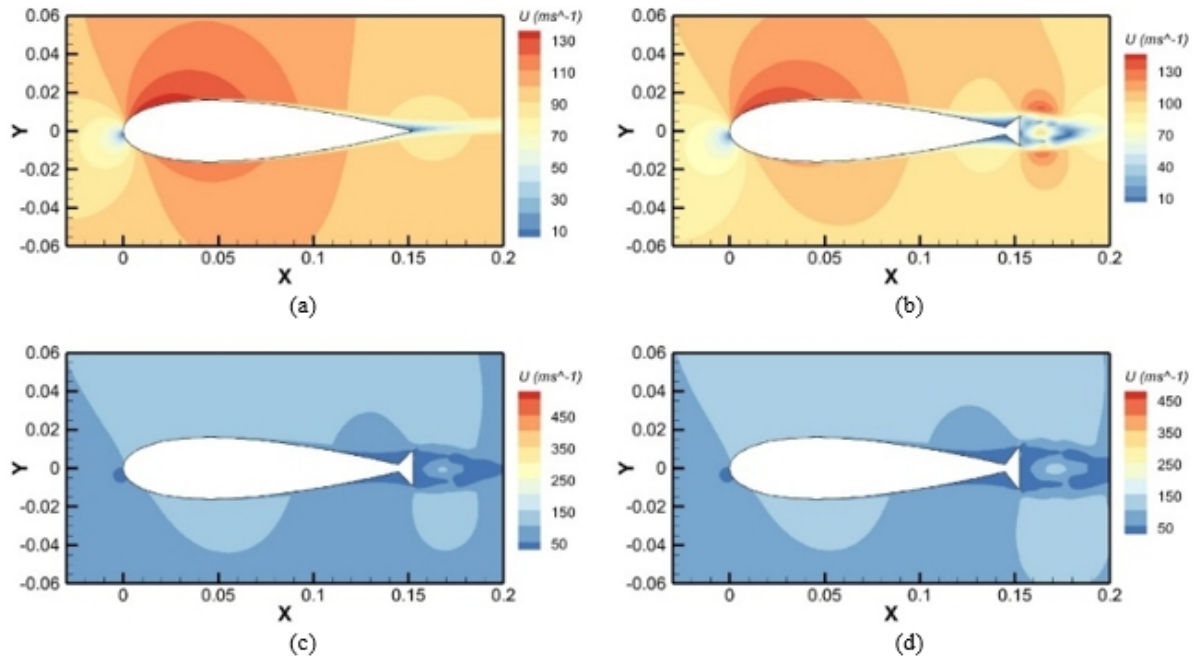
Source: Authors.

Figure 8: Percent increase in (a) lift coefficient ( $C_L$ ) and (b) drag coefficient ( $C_D$ ) with respect to NACA 0021 airfoil as a function of Mach number ( $M$ ) at  $3^\circ$  angle of attack ( $\alpha$ ).



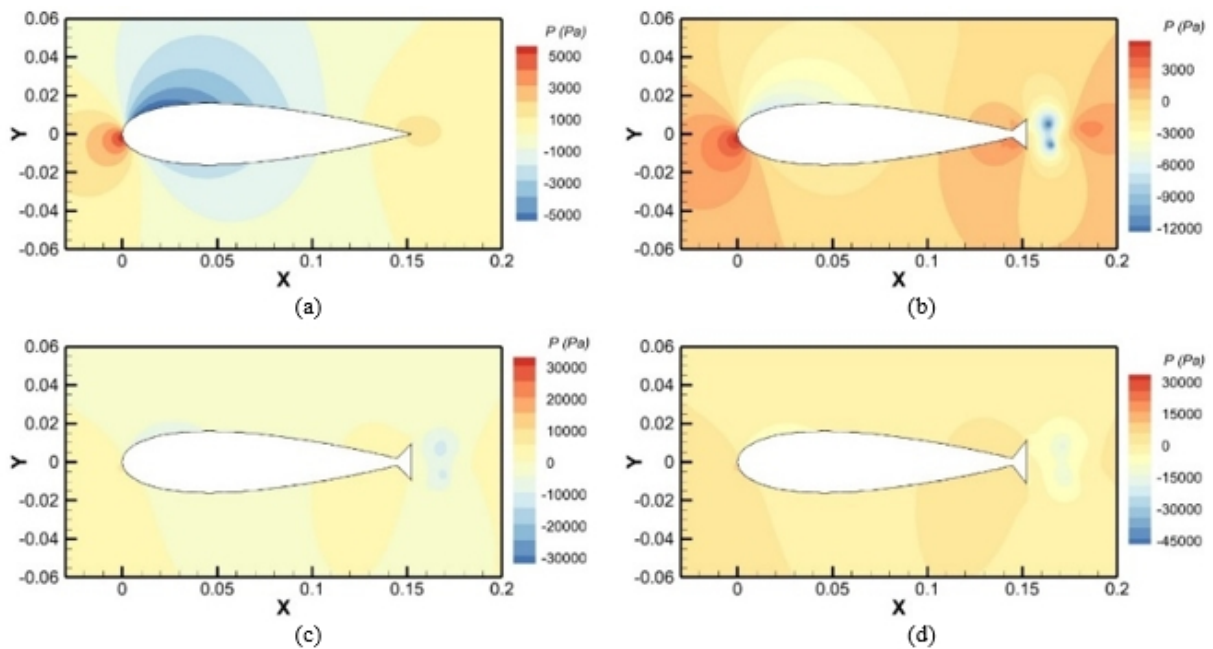
Source: Authors.

Figure 9: Velocity contours of the (a) NACA 0021 (b) Wedge tail 01 (c) Wedge tail 02 (d) Wedge tail 03 airfoil at  $3^\circ$  angle of attack ( $\alpha$ ) with a Reynolds number ( $Re$ ) of  $1 \times 10^6$ .



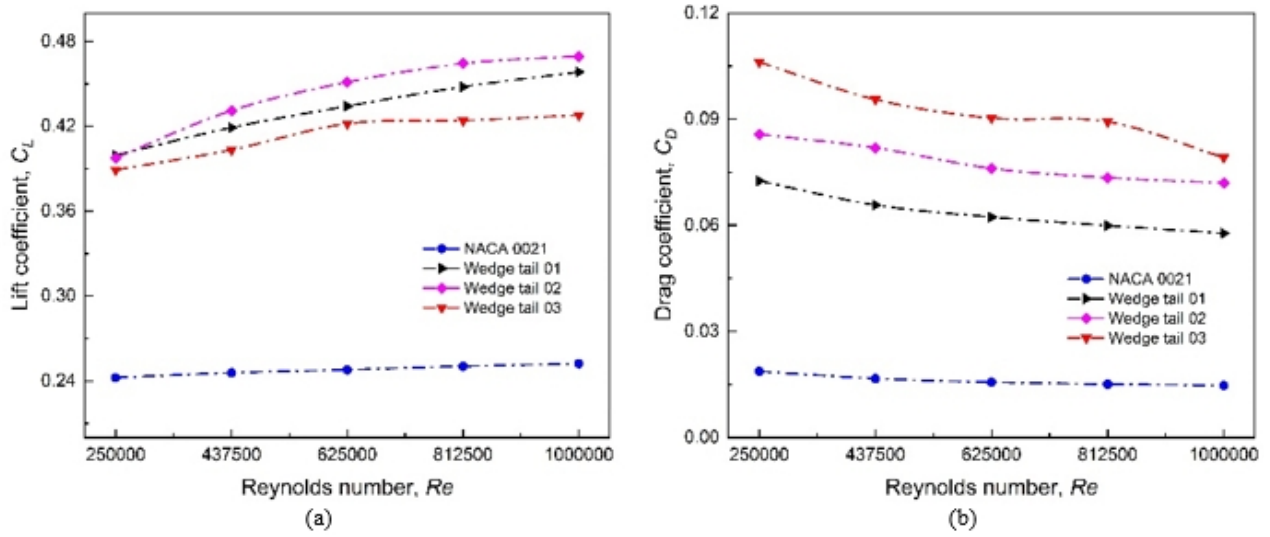
Source: Authors.

Figure 10: Pressure contours of the (a) NACA 0021 (b) Wedge tail 01 (c) Wedge tail 02 (d) Wedge tail 03 airfoil at  $3^\circ$  angle of attack ( $\alpha$ ) with a Reynolds number ( $Re$ ) of  $1 \times 10^6$ .



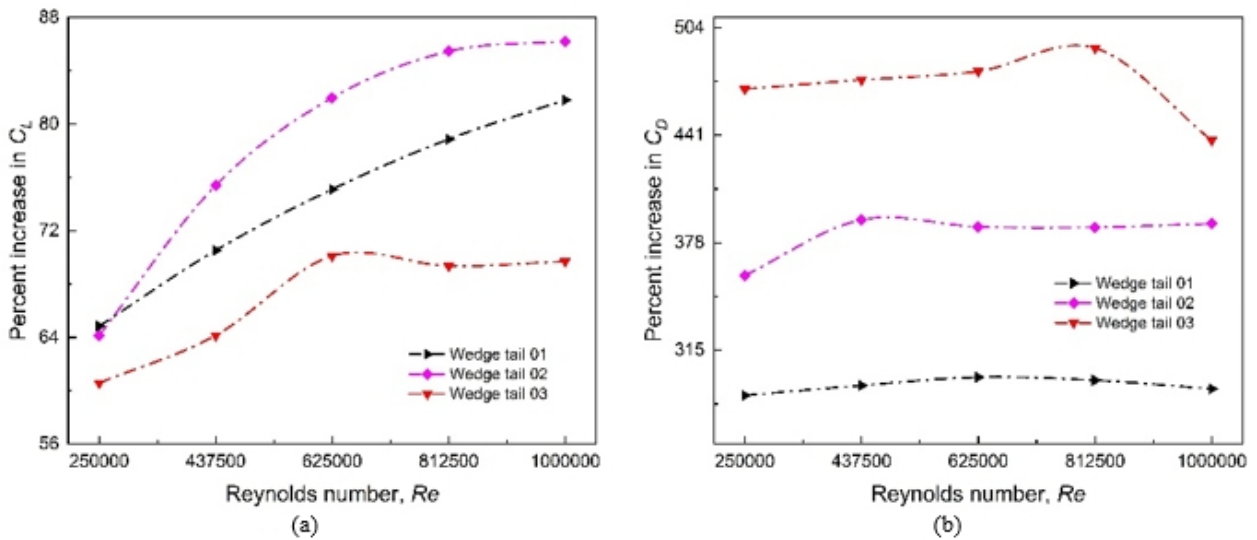
Source: Authors.

Figure 11: (a) Lift coefficient ( $C_L$ ) and (b) drag coefficient ( $C_D$ ) as a function of Reynolds number ( $Re$ ) at  $3^\circ$  angle of attack ( $\alpha$ ).



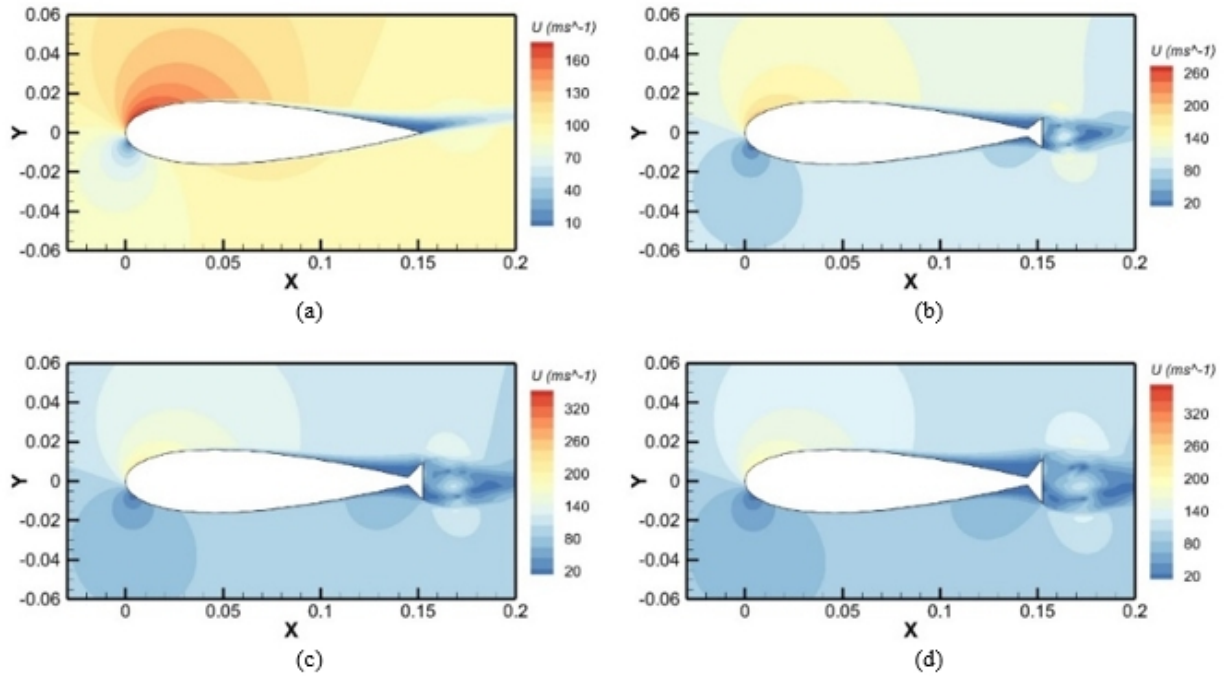
Source: Authors.

Figure 12: Percent increase in (a) lift coefficient ( $C_L$ ) and (b) drag coefficient ( $C_D$ ) with respect to NACA 0021 airfoil as a function of Reynolds number ( $Re$ ) at  $3^\circ$  angle of attack ( $\alpha$ ).



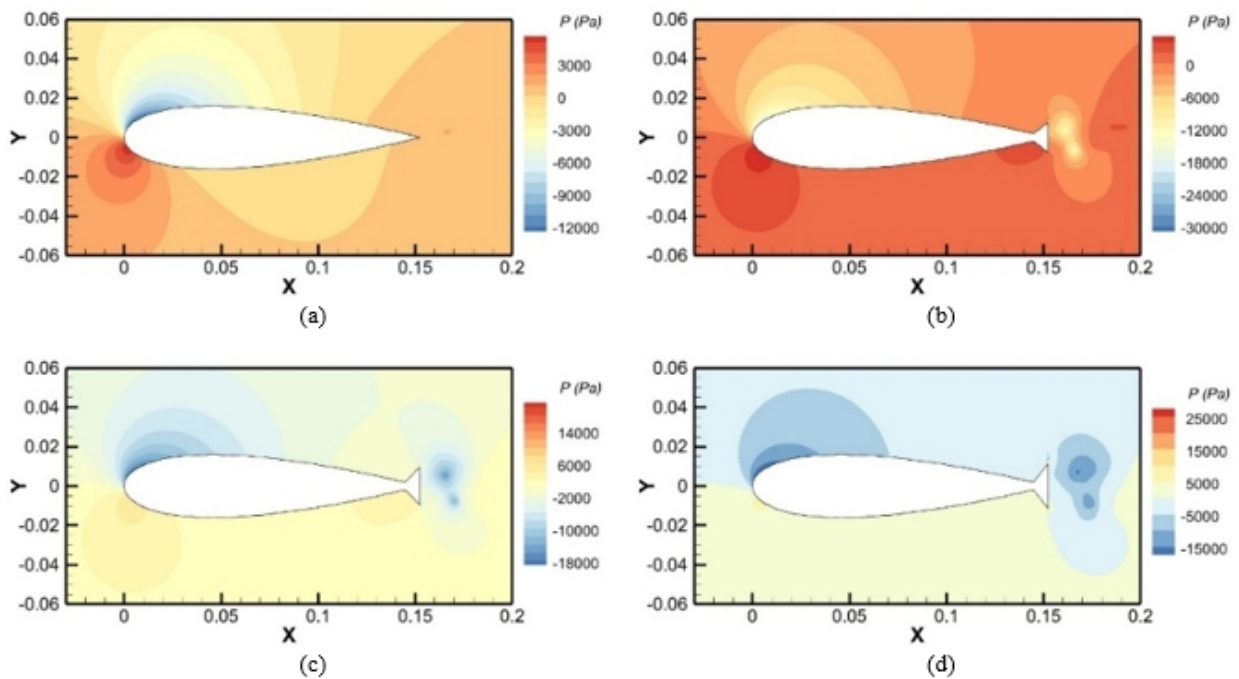
Source: Authors.

Figure 13: Velocity contours of the (a) NACA 0021 (b) Wedge tail 01 (c) Wedge tail 02 (d) Wedge tail 03 airfoil at  $9^\circ$  angle of attack ( $\alpha$ ) with a Reynolds number ( $Re$ ) of  $1 \times 10^6$ .



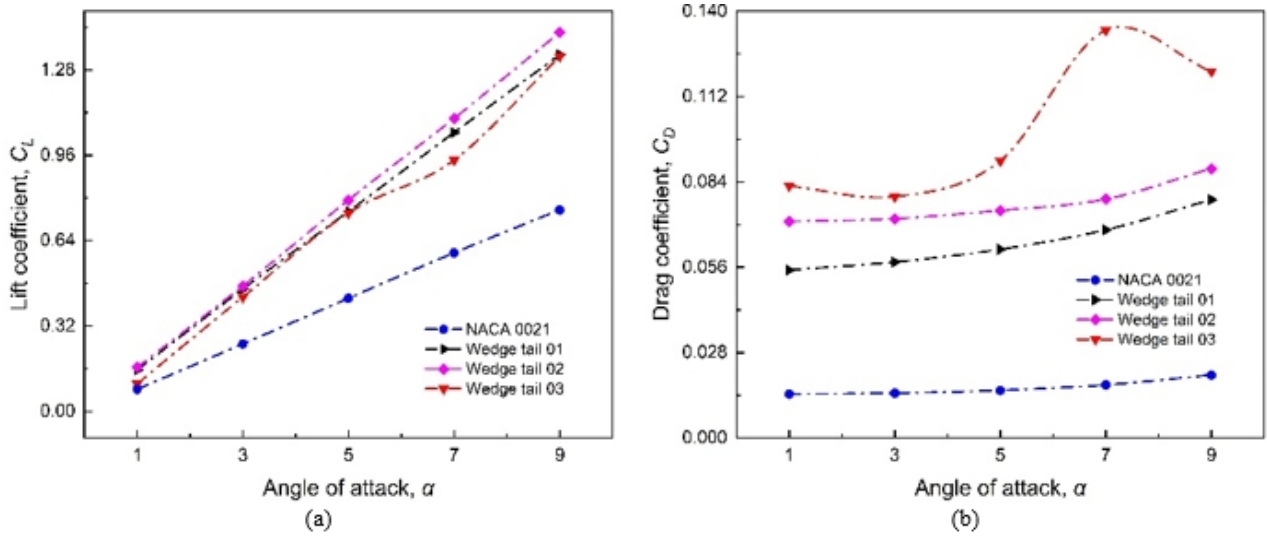
Source: Authors.

Figure 14: Pressure contours of the (a) NACA 0021 (b) Wedge tail 01 (c) Wedge tail 02 (d) Wedge tail 03 airfoil at  $9^\circ$  angle of attack ( $\alpha$ ) with a Reynolds number ( $Re$ ) of  $1 \times 10^6$ .



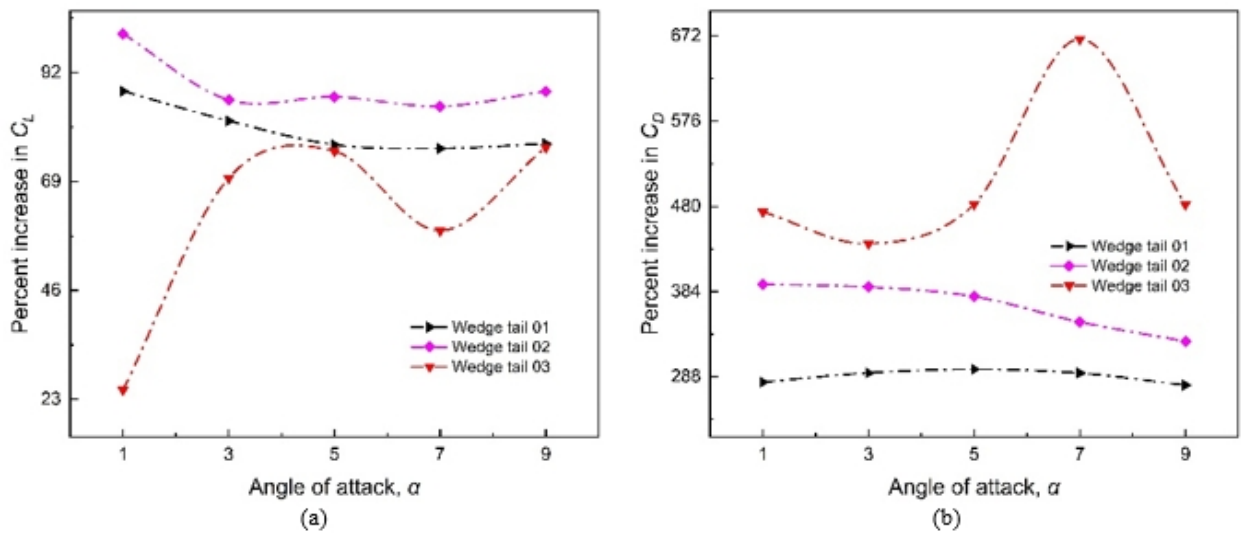
Source: Authors.

Figure 15: (a) Lift coefficient ( $C_L$ ) and (b) drag coefficient ( $C_D$ ) as a function of angle of attack ( $\alpha$ ) at Reynolds number ( $Re$ ) of  $1 \times 10^6$ .



Source: Authors.

Figure 16: Percent increase in (a) lift coefficient ( $C_L$ ) and (b) drag coefficient ( $C_D$ ) with respect to NACA 0021 airfoil as a function of angle of attack ( $\alpha$ ) at Reynolds number ( $Re$ ) of  $1 \times 10^6$ .



Source: Authors.

effects of the angle of attack on velocity, pressure, lift coefficient, and drag coefficient for four different airfoils is presented in Figs. 13, 14, and 15, respectively. Fig. 15 shows that Wedge Tail 02 has the highest lift coefficient, increasing with the angle of attack. In contrast, NACA 0021 airfoil has the lowest drag coefficient, increasing with an increase in angle of attack. Additionally, the wedge tail thickness has a considerable effect on the lift coefficient and drag coefficient, as demonstrated in Fig. 16.

## Conclusions.

The objective of this study was to analyze the effect of a wedge tail thickness on the performance of the NACA 0021 airfoil. To achieve this, RANS-based CFD simulations were conducted in a two-dimensional domain using the  $k - \omega$  SST turbulence model to determine the lift coefficient and drag coefficient of the airfoils. The study also investigated the effects of the Mach numbers, Reynolds numbers, and angle of attack on the performance of airfoils. The results of the study indicate that both lift and drag coefficients increased with an increase in the angle of attack, while an increase in Mach and Reynolds numbers led to a decrease in drag coefficient and an increase in lift coefficient. Furthermore, the inclusion of a wedge tail had a positive effect on the lift coefficients but a negative effect on the drag coefficients. The NACA 0021 airfoil with a wedge tail thickness of 12.5% of the chord length of the airfoil has demonstrated the highest percentage of lift coefficient increase, ranging from 60% ~ 100%. In contrast, wedge tail thickness of 15% of the chord length of the airfoil showed the highest percentage of drag coefficient increase, ranging from 435% ~ 670%. Overall, this study provides valuable insights into the design and optimization of airfoils for improved aerodynamic performance.

## References.

- Douvi, C. E., Tsavalos, I. A., Margaris, P. D., 2012. Evaluation of the turbulence models for the simulation of the flow over a national advisory committee for aeronautics (naca) 0012 airfoil. *Journal of Mechanical Engineering Research* 4 (3), 100–111.
- Fernández, A., Chakkor, M. R., 2006. Airfoil section optimization for use in sailboat foils. *Journal of Maritime Research* 3 (3), 53–68.
- Frei, W., 2017. Which turbulence model should i choose for my cfd application? *Cmsol Blog*, 1–8.
- Hoerner, S. F., Borst, H. V., 1975. *Fluid dynamic lift*, published by mrs. Liselotte A. Hoerner.
- Holst, D., Church, B., Wegner, F., Pechlivanoglou, G., Nayeri, C., Paschereit, C., 2019. Experimental analysis of a naca 0021 airfoil under dynamic angle of attack variation and low reynolds numbers. *Journal of Engineering for Gas Turbines and Power* 141 (3).
- Liu, J., Hekkenberg, R., 2015. Hydrodynamic characteristics of twin-rudders at small attack angles. In: *IMDC 2015: Proceedings of the 12th International Marine Design Conference*, Tokyo, Japan, 11-14 May 2015. Citeseer.
- Menter, F. R., 1994. Two-equation eddy-viscosity turbulence models for engineering applications. *AIAA journal* 32 (8), 1598–1605.
- Molland, A. F., 2011. *The maritime engineering reference book: a guide to ship design, construction and operation*. Elsevier.
- Molland, A. F., Turnock, S. R., 2011. *Marine rudders and control surfaces: principles, data, design and applications*. Elsevier.
- Nguyen, T., Ikeda, Y., 11 2014. Hydrodynamic characteristics of rudder sections with high lift force (part 3). DOI: 10.13140/RG.2.1.1306.2889
- Nguyen, T., Ikeda, Y., 2016. Hydrodynamic characteristics of high lift rudders with wedge tails. *Proceeding of APHydro2016*, 238–245.
- Rostamzadeh, N., Hansen, K., Kelso, R., Dally, B., 2014. The formation mechanism and impact of streamwise vortices on naca 0021 airfoil's performance with undulating leading edge modification. *Physics of Fluids* 26 (10), 107101.
- Rostamzadeh, N., Kelso, R., Dally, B., Hansen, K., 2013. The effect of undulating leading-edge modifications on naca 0021 airfoil characteristics. *Physics of fluids* 25 (11), 117101.
- Sener, M. Z., Aksu, E., 2022. The numerical investigation of the rotation speed and reynolds number variations of a naca 0012 airfoil. *Ocean Engineering* 249, 110899.
- Sheldahl, R. E., Klimas, P. C., 1981. *Aerodynamic characteristics of seven symmetrical airfoil sections through 180-degree angle of attack for use in aerodynamic analysis of vertical axis wind turbines*. Tech. rep., Sandia National Labs., Albuquerque, NM (USA).
- Suvanjumrat, C., 06 2017. Comparison of turbulence models for flow past naca0015 airfoil using openfoam. *Engineering Journal* 21, 207–221. DOI: 10.4186/ej.2017.21.3.207
- Tasif, T. H., Karim, M. M., 2017. Effect of fish wedge on the hydrodynamic characteristics of a marine rudder. *Procedia engineering* 194, 136–143.
- Thieme, H., 1965. *Design of ship rudders (zur formgebung von schiffsrudern)*. Tech. rep., DAVID TAYLOR MODEL BASIN WASHINGTON DC.
- Tuncer, I. H., Platzer, M. F., 2000. Computational study of flapping airfoil aerodynamics. *Journal of aircraft* 37 (3), 514–520.
- Van, N. T., Yoshiho, I., 2015. A development of high lift rudder sections. (1 (22)), 14–21.
- Van Nguyen, T., Ikeda, Y., 2013. Hydrodynamic characteristic of rudder sections with high lift force. *J Jpn Soc Nav Arch Ocean Eng*, 403–406.
- Van Nguyen, T., Ikeda, Y., 2014a. Development of fishtail rudder sections with higher maximum lift coefficients. In: *The Twenty-fourth International Ocean and Polar Engineering Conference*. OnePetro.

Van Nguyen, T., Ikeda, Y., 2014b. Hydrodynamic characteristic of rudder sections with high lift force (part 2). In: Proceedings of The Japan Society of Naval Architects and Ocean Engineers (JASNAOE) Annual Spring Meeting, Sendai, Japan.

Versteeg, H. K., Malalasekera, W., 2007. An introduction to computational fluid dynamics: the finite volume method. Pearson education.